Article

# Anisotropic In-Plane Gradients of Poly(acrylic acid) Formed by Electropolymerization with Spatiotemporal Control of the Electrochemical Potential

Xuejun Wang, and Paul W. Bohn

*J. Am. Chem. Soc.*, **2004**, 126 (21), 6825-6832• DOI: 10.1021/ja0400436 • Publication Date (Web): 05 May 2004



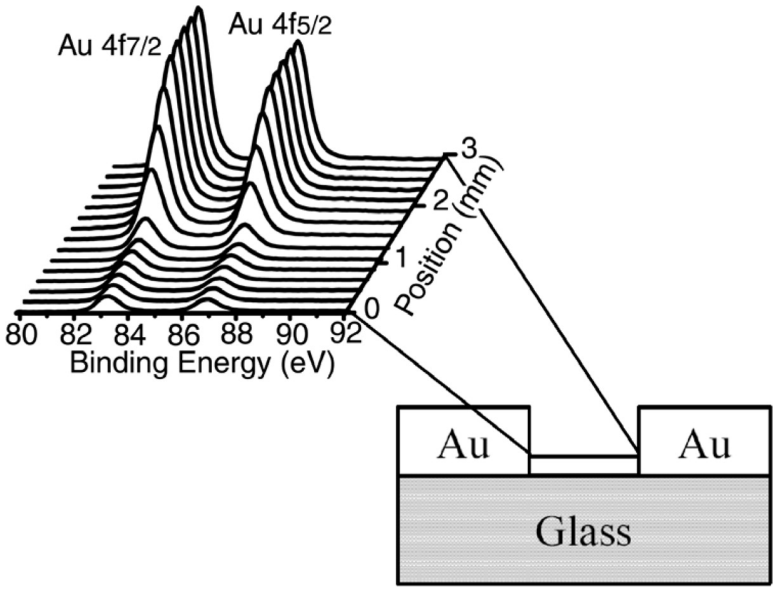


## More About This Article

Additional resources and features associated with this article are available within the HTML version:

- Supporting Information
- Links to the 5 articles that cite this article, as of the time of this article download
- Access to high resolution figures
- Links to articles and content related to this article
- Copyright permission to reproduce figures and/or text from this article

View the Full Text HTML

J|A|C|S
ARTICLES
Published on Web 05/05/2004

# Anisotropic In-Plane Gradients of Poly(acrylic acid) Formed by Electropolymerization with Spatiotemporal Control of the Electrochemical Potential

Xuejun Wang and Paul W. Bohn*

*Contribution from the Department of Chemistry and Frederick Seitz Materials Research Laboratory, University of Illinois at Urbana-Champaign, 600 South Mathews Avenue, Urbana, Illinois 61801*

Received February 5, 2004; E-mail: bohn@scs.uiuc.edu

***Abstract:*** Laterally varying thickness gradients of poly(acrylic acid) (PAA) were formed by Zn(II)-catalyzed electropolymerization of acrylic acid (AA) in the presence of an in-plane electrochemical potential gradient applied to Au working electrodes. In the static potential gradient (SPG) approach, two ends of a Au working electrode were clamped at distinct potentials for the duration of the electropolymerization process, thereby generating a time-independent in-plane electrochemical potential gradient, $V(x)$. A dynamic potential gradient (DPG) approach was also used, in which the two end potentials were varied in time, while maintaining a constant voltage offset, to generate an in-plane electrochemical potential gradient, $V(x,t)$. Because the kinetics of heterogeneous electron transfer vary with the local overpotential, these two methods produce PAA films with laterally varying thickness gradients, although they exhibit different spatial characteristics. X-ray photoelectron spectroscopy (XPS) and surface plasmon resonance (SPR) imaging were used to characterize the PAA gradients. The in-plane thickness variations of PAA gradients formed by both SPG and DPG approaches agree with predictions of the Butler−Volmer equation at small absolute overpotentials, while at large (negative) overpotentials, mass transport dominates, and the thickness reaches a plateau value independent of local potential. DPG-produced PAA gradients are generally broader than SPG gradients with the same initial potential and comparable effective growth time, indicating that the DPG approach is more suitable for formation of thicker gradients.

## Introduction

Recently there has been a great deal of interest in generating and utilizing laterally anisotropic (gradient) surfaces for a variety of reasons: to achieve structures that interact with their environment in a spatially directional manner, for their practical utility in selective adsorption experiments, as templates for cell migration, and as tools for continuous readout of surface−environment interactions. Chemical composition gradients[1−13] and gradients of physical properties, e.g., morphology,[14] density,[15] catalytic activity,[16] porosity,[17] and nanowire length,[18] have all been experimentally realized. A number of techniques have been exploited to generate gradients on various substrates, including diffusion-controlled vapor deposition,[1] cross diffusion,[2,3] corona discharge,[10,11] photoimmobilization,[12,13] the use of microfluidic devices,[7,8] and, more recently, scanning tunneling microscopy (STM)-based replacement lithography.[9]

In our laboratory, an approach based on spatial gradients of electrochemical potential at ultrathin Au electrodes has been used to generate chemical composition gradients.[5,6,19−23] In this

(1) Chaudhury, M. K.; Whitesides, G. M. *Science* **1992**, *256*, 1539−1541.
(2) Liedberg, B.; Tengvall, P. *Langmuir* **1995**, *11*, 3821−3827.
(3) Liedberg, B.; Wirde, M.; Tao, Y.-T.; Tengvall, P.; Gelius, U. *Langmuir* **1997**, *13*, 5329−5334.
(4) Ruardy, T. G.; Schakenraad, J. M.; van der Mei, H. C.; Busscher, H. J. *Surf. Sci. Rep.* **1997**, *29*, 1−30.
(5) Terrill, R. H.; Balss, K. M.; Zhang, Y.; Bohn, P. W. *J. Am. Chem. Soc.* **2000**, *122*, 988−989.
(6) Balss, K. M.; Coleman, B. D.; Lansford, C. H.; Haasch, R. T.; Bohn, P. W. *J. Phys. Chem. B* **2001**, *105*, 8970−8978.
(7) Jeon, N. L.; Dertinger, S. K. W.; Chiu, D. T.; Choi, I. S.; Stroock, A. D.; Whitesides, G. M. *Langmuir* **2000**, *16*, 8311−8316.
(8) Dertinger, S. K. W.; Jiang, X.; Li, Z.; Murthy, V. N.; Whitesides, G. M. *Proc. Natl. Acad. Sci. U.S.A.* **2002**, *99*, 12542−12547.
(9) Fuierer, R. R.; Carroll, R. L.; Feldheim, D. L.; Gorman, C. B. *Adv. Mater.* **2002**, *14*, 154−157.
(10) Jeong, B. J.; Lee, J. H.; Lee, H. B. *J. Colloid Interface Sci.* **1996**, *178*, 757−763.
(11) Lee, J. H.; Kim, H. G.; Khang, G. S.; Lee, H. B.; Jhon, M. S. *J. Colloid Interface Sci.* **1992**, *151*, 563−570.
(12) Hypolite, C. L.; McLernon, T. L.; Adams, D. N.; Chapman, K. E.; Herbert, C. B.; Huang, C. C.; Distefano, M. D.; Hu, W.-S. *Bioconjugate Chem.* **1997**, *8*, 658−663.
(13) Herbert, C. B.; McLernon, T. L.; Hypolite, C. L.; Adams, D. N.; Pikus, L.; Huang, C. C.; Fields, G. B.; Letourneau, P. C.; Distefano, M. D.; Hu, W.-S. *Chem. Biol.* **1997**, *4*, 731−737.
(14) Einaga, Y.; Kim, G. S.; Ohnishi, K.; Park, S. G.; Fujushima, A. *Mater. Sci. Eng., B* **2001**, *83*, 19−23.
(15) Wu, T.; Efimenko, K.; Vlcek, P.; Subr, V.; Genzer, J. *Macromolecules* **2003**, *36*, 2448−2453.
(16) Jayaraman, S.; Hillier, A. C. *Langmuir* **2001**, *17*, 7857−7864.
(17) Neubrand, A. *J. Appl. Electrochem.* **1998**, *28*, 1179−1188.
(18) Sehayek, T.; Vaskevich, A.; Rubinstein, I. *J. Am. Chem. Soc.* **2003**, *125*, 4718−4719.
(19) Balss, K. M.; Fried, G. A.; Bohn, P. W. *J. Electrochem. Soc.* **2002**, *149*, C450−C455.
(20) Balss, K. M.; Kuo, T.-C.; Bohn, P. W. *J. Phys. Chem. B* **2003**, *107*, 994−1000.
(21) Plummer, S. T.; Wang, Q.; Bohn, P. W.; Stockton, R.; Schwartz, M. A. *Langmuir* **2003**, *19*, 7528−7536.
(22) Plummer, S. T.; Bohn, P. W. *Langmuir* **2002**, *18*, 4142−4149.

method, current is injected at one end of an ultrathin (5 nm ≤ $d$ ≤ 80 nm) Au film and collected at the other end, while the Au film is used simultaneously as the working electrode of an electrochemical cell. Injecting current yields a significant in-plane potential drop so that, rather than assuming a single value of potential, an in-plane potential gradient, $V(x)$, is imposed on the working electrode surface, according to

$$V(x) = V_0 + \int_0^x \frac{i\rho(l)}{A} dl \quad (1)$$

where $V_0$ is the potentiostat voltage offset, $i$ is the magnitude of the injected current, $A$ is the cross-sectional area of the Au working electrode, and $\rho(l)$ is the position-dependent film resistivity given by

$$\rho(l) = \rho_0 + \delta(l) + \kappa\Gamma(l) \quad (2)$$

where $\rho_0$ is the bulk resistivity, $\delta(l)$ is a stochastic term associated with variations in the film morphology, $\kappa$ is an adsorbate-dependent constant, and $\Gamma(l)$ is the local adsorbate coverage. However, the stochastic and adsorption terms typically produce an effect ≤1 to 2%, and thus they can be neglected for all but the most precise applications.[5]

The in-plane potential gradient can be exploited to map heterogeneous electron-transfer reactions onto the Au electrode surface, as demonstrated, for example, with the characteristic reductive desorption/oxidative adsorption reactions of alkanethiols.[24−30] In contrast to other gradient preparation methods, this approach allows gradient properties, such as transition position and slope, to be controlled in both space and time. Furthermore, any electrochemical reaction that alters the strength or mode of surface interaction with its environment[31,32] may be anisotropically displayed by exploiting in-plane electrochemical potential gradients. For example, Hillier and Jayaraman formed gradients of Pt catalyst coverage on an electrically conductive indium−tin−oxide (ITO),[16] and Rubinstein et al. fabricated arrays of templated nanowires with laterally varying length by exploiting spatiotemporal control of in-plane potentials.[18]

In the present work, an electrochemical potential gradient approach is applied to vary a physical property (PAA thickness) while leaving composition unaltered. Laterally varying nanometer-scale thickness gradients of poly(acrylic acid) (PAA) are fabricated by Zn(II)-catalyzed electropolymerization of acrylic acid (AA) in the presence of an in-plane electrochemical potential gradient, used here to control the local rate of electropolymerization.[33−36] Polymer hydrogels, such as PAA, are of interest because they can change their volume and shape reversibly, in response to external stimuli, such as temperature, solvent composition, pH, ionic concentration, electric field, and light.[37−48] They are promising materials for bio-actuators,[49−51] e.g., artificial muscles and lenses and vitreous bodies in ophthalmology, and for chemical and biochemical sensors, based on either direct analyte-induced volume changes[52−57] or as scaffolds for molecular recognition agents.[58,59] Clearly lateral control over film thickness would open up the possibility of continuous readout in sensing applications and more adaptable control of actuation.[60]

In the course of applying the electrochemical potential gradient approach to the electropolymerization of AA, a new mode of gradient formation is explored. In contrast to the static potential gradients (SPG) described by eq 1, it is possible to create laterally varying in-plane properties using dynamic potential gradients (DPG). In this approach, the two end potentials are varied in time, while maintaining a constant offset, to generate an in-plane electrochemical potential gradient, $V(x,t)$, according to

$$V(x, t) = V_0(t) + \int_0^x \frac{i\rho(l)}{A} dl \quad (3)$$

The kinetics of heterogeneous electron-transfer reactions generally, and electropolymerization specifically, vary with the local overpotential. The SPG and DPG approaches produce different


(23) Wang, Q.; Jakubowski, J. A.; Sweedler, J. V.; Bohn, P. W. *Anal. Chem.* **2004**, *76*, 1−8.
(24) Stevenson, K.; Mitchell, M.; White, H. *J. Phys. Chem. B* **1998**, *102*, 1235.
(25) Hatchett, D. W.; Uibel, R. H.; Stevenson, K. J.; Harris, J. M.; White, H. S. *J. Am. Chem. Soc.* **1998**, *120*, 1062−1069.
(26) Widrig, C. A.; Chung, C.; Porter, M. D. *J. Electroanal. Chem.* **1991**, *310*, 335−359.
(27) Walczak, M. M.; Popenoe, D. D.; Deinhammer, R. S.; Lamp, B. D.; Chung, C.; Porter, M. D. *Langmuir* **1991**, *7*, 2687−2693.
(28) Vinokurov, I. A.; Morin, M.; Kankare, J. *J. Phys. Chem. B* **2000**, *104*, 5790−5796.
(29) Yang, D.; Wilde, C.; Morin, M. *Langmuir* **1997**, *13*, 243−249.
(30) Yang, D.; Al-Maznai, H.; Morin, M. *J. Phys. Chem. B* **1997**, *101*, 1158−1166.
(31) Yeo, W. S.; Yousaf, M. N.; Mrksich, M. *J. Am. Chem. Soc.* **2003**, *125*, 14994−14995.
(32) Jiang, X. Y.; Ferrigno, R.; Mrksich, M.; Whitesides, G. M. *J. Am. Chem. Soc.* **2003**, *125*, 2366−2367.
(33) Collins, G. L.; Thomas, N. W. *J. Polym. Sci., Polym. Chem. Ed.* **1977**, *15*, 1819−1831.
(34) Katz, E.; de Lacey, A. L.; Fierro, J.; Palacios, J. M.; Fernandez, V. M. *J. Electroanal. Chem.* **1993**, *358*, 247−259.
(35) Chegel, V.; Raitman, O. A.; Lioubashevski, O.; Shirshov, Y.; Willner, I. *Adv. Mater.* **2002**, *14*, 1549−1553.
(36) Gabai, R.; Sallacan, N.; Chegel, V.; Bourenko, T.; Katz, E.; Willner, I. *J. Phys. Chem. B* **2001**, *105*, 8196−8202.
(37) Berndt, I.; Richtering, W. *Macromolecules* **2003**, *36*, 8780−8785.
(38) Kishi, R.; Miura, T.; Kihara, H.; Asano, T.; Shibata, M.; Yosomiya, R. *J. Appl. Polym. Sci.* **2003**, *89*, 75−84.
(39) Park, J. S.; Lee, H. J.; Choi, S. J.; Geckeler, K. E.; Cho, J.; Moon, S. H. *J. Colloid Interface Sci.* **2003**, *259*, 293−300.
(40) Yamashita, K.; Hashimoto, O.; Nishimura, T.; Nango, M. *React. Funct. Polym.* **2002**, *51*, 61−68.
(41) Katime, I.; Rodriguez, E. *J. Macromol. Sci., Pure Appl. Chem.* **2001**, *38*, 543−558.
(42) Dautzenberg, H.; Gao, Y. B.; Hahn, M. *Langmuir* **2000**, *16*, 9070−9081.
(43) Chiu, H. C.; Yang, C. H. *Polym. J.* **2000**, *32*, 574−582.
(44) White, B. H. B.; Kwak, J. C. T. *Colloid Polym. Sci.* **1999**, *277*, 785−791.
(45) Otake, K.; Karaki, R.; Ebina, T.; Yokoyama, C.; Takahashi, S. *Macromolecules* **1993**, *26*, 2194−2197.
(46) Kawasaki, H.; Sasaki, S.; Maeda, H. *J. Phys. Chem. B* **1997**, *101*, 5089−5093.
(47) Qiu, Y.; Park, K. *Adv. Drug Delivery Rev.* **2001**, *53*, 321−339.
(48) Kim, S. J.; Lee, K. J.; Kim, S. I.; Lee, Y. M.; Chung, T. D.; Lee, S. H. *J. Appl. Polym. Sci.* **2003**, *89*, 2301−2305.
(49) Arndt, K. F.; Richter, A.; Ludwig, S.; Zimmermann, J.; Kressler, J.; Kuckling, D.; Adler, H. J. *Acta Polym.* **1999**, *50*, 383−390.
(50) Karlsson, J. O.; Gatenholm, P. *Polymer* **1999**, *40*, 379−387.
(51) Suzuki, M.; Hirasa, O. *Adv. Polym. Sci.* **1993**, *110*, 241−261.
(52) Ruan, C. M.; Zeng, K. F.; Grimes, C. A. *Anal. Chim. Acta* **2003**, *497*, 123−131.
(53) Hilt, J. Z.; Gupta, A. K.; Bashir, R.; Peppas, N. A. *Biomed. Microdevices* **2003**, *5*, 177−184.
(54) Chong, K. T.; Su, X. D.; Lee, E. J. D.; O'Shea, S. J. *Langmuir* **2002**, *18*, 9932−9936.
(55) Chabukswar, V. V.; Pethkar, S.; Athawale, A. A. *Sens. Actuators, B* **2001**, *77*, 657−663.
(56) Athawale, A. A.; Chabukswar, V. V. *J. Appl. Polym. Sci.* **2001**, *79*, 1994−1998.
(57) Cai, Q. Y.; Grimes, C. A. *Sens. Actuators, B* **2000**, *71*, 112−117.
(58) Pardo-Yissar, V.; Katz, E.; Lioubashevski, O.; Willner, I. *Langmuir* **2001**, *17*, 1110−1118.
(59) Raitman, O. A.; Katz, E.; Buckmann, A. F.; Willner, I. *J. Am. Chem. Soc.* **2002**, *124*, 6487−6496.
(60) Suchaneck, G.; Guenther, M.; Sorber, J.; Gerlach, G.; Arndt, K.-F.; Deyneka, A.; Jastrabik, L. *Surf. Coat. Technol.* **2003**, *174−175*, 816−820.

$V(x,t)$ profiles and, thus, should produce PAA thickness gradients with different properties. The fabrication and characterization of PAA thickness gradients produced by these two electrochemical gradients approaches are explored here.

## Experimental Section

**Materials.** 11-Mercaptoundecanoic acid (MUA), acrylic acid, *N*,*N*′-methylenebisacrylamide, and zinc chloride were purchased from Aldrich. KOH and HCl were purchased from Fischer Scientific. Absolute ethanol (EtOH) was purchased from Aaper Alcohol and Chemical Company. All reagents were used as received.

**Substrate Preparation.** Microscope slides, cut into 13 mm by 8 mm pieces, and 60° SF-10 prisms (Spindler & Hoyer) were cleaned in piranha solution (concentrated $H_2SO_4$ and 30% $H_2O_2$ 3:1 in volume. *CAUTION: piranha solutions are strongly oxidizing and should not be allowed to contact organic solvents*.) for 30 min, and then were rinsed completely with copious amounts of deionized (18.2 MΩ cm) $H_2O$. Cleaned samples were transferred to the evaporation chamber immediately to minimize contamination. The pressure in the vacuum chamber was maintained below $5 \times 10^{-8}$ Torr during evaporation. The electrode preparation was accomplished in two steps. First, two 150-nm thick Au pads (3 mm × 3 mm) separated by 3 mm were evaporated on a glass substrate. Then, a 50-nm thick Au stripe was evaporated over the Au pads to generate a 3 mm × 1 mm active region for gradient formation. An adhesion layer of Cr (1 nm) was deposited under each layer of Au. The deposition rates for Cr and Au were 0.03 Å/s and 1.5 Å/s, respectively. Samples were stored under $N_2$ before use. Prior to polymer formation, the Au substrates were cleaned in piranha solution for 1 min, rinsed thoroughly with deionized $H_2O$, rinsed again with EtOH, and blown dry with $N_2$. For surface plasmon resonance (SPR) imaging experiments, two 150-nm thick Au pads separated by 25 mm were first evaporated on the prisms to maintain good contact. Then 45 nm of Au with a 1-nm Cr adhesion layer were deposited over the Au pads. The active gradient formation area was defined by a 12.5-mm diameter O-ring that sealed the cell. Prior to polymer formation, the films were exposed to $O_3$ for 25 min, rinsed thoroughly with EtOH, and dried with $N_2$. $O_3$ was produced by passing $O_2$ at low flow rate past a UV-emitting Hg lamp upstream of the sample chamber.

**Gradient Formation.** To prepare the gradients, a bipotentiostat was connected to the two ends of a Au thin film working electrode in a cell employing a saturated Ag/AgCl reference electrode and a stainless steel counter electrode in an aqueous solution of 2.0 M acrylic acid, 0.04 M *N*,*N*′-methylenebisacrylamide, and 0.2 M $ZnCl_2$. Contacts were made on opposite ends of the rectangular thin film working electrode by pressing Au wires onto thick Au pads which served as working electrodes $E_1$ and $E_2$, viz. Figure 1a. Typically, static PAA thickness gradients were formed using SPG potential programs by setting ($E_1$, $E_2$) = (−1.3 V, −1.1 V) for 5 or 10 s. DPG-derived PAA thickness gradients were formed by applying a triangular potential sweep $E_1(t)$ while maintaining a constant potential offset, $\Delta = (E_2 - E_1)$ throughout the experiment (Figure 1b). For Au-covered glass samples, $E_1$ was cycled between −1.5 and 0 V five times, keeping $\Delta = +300$ mV throughout the experiment. For SPR imaging experiments, contacts were made to two thick Au pads as above, and $E_1$ was swept from −1.4 to 0 V, keeping a $\Delta = +400$ mV offset throughout the experiment. Because the working electrode connections were made outside of the solution volume defined by the O-ring seal, the potential program in the active PAA formation area resulted in a sweep from −1.3 to +0.1 V at one edge of the cell and from −1.1 to +0.3 V at the other end. Narrow ($\Delta = 200$ mV) dynamic potential windows were used for SPR imaging experiments to probe the transition region more effectively. For comparison, a static PAA gradient on the Au/prism surface was formed by applying ($E_1$, $E_2$) = (−1.3 V, −1.1 V) while imaging with SPR. After gradient film formation, samples were treated with 0.1 M HCl for 10 min., sonicated in 0.1 M HCl for 30 s, rinsed with deionized $H_2O$ for 30 s, and blown dry with $N_2$.

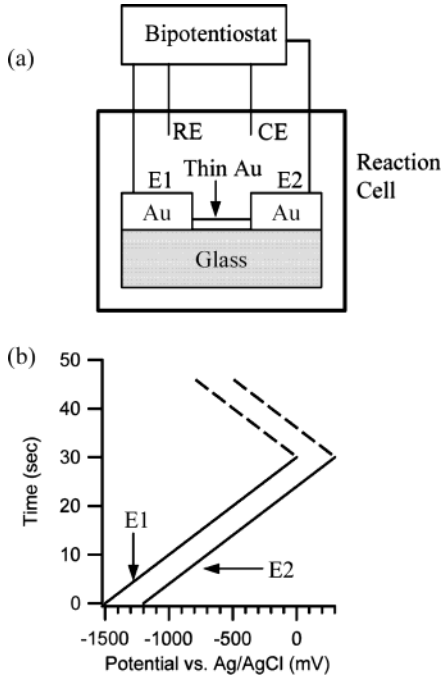


***Figure 1.*** (a) Schematic illustration of electrochemical gradient formation scheme on a Au/glass sample. A bipotentiostat applies potentials ($E_1$, $E_2$) to two thick Au pads at opposite ends of the ultrathin Au film, which forms the active gradient-formation region. (b) Dynamic potential gradient formation strategy. A triangular potential sweep $E_1(t)$ is applied while maintaining the potential offset, $\Delta = (E_2 - E_1)$ constant.

**X-ray Photoelectron Spectroscopy (XPS).** X-ray photoelectron spectra were obtained using a Kratos Axis ULTRA spectrometer with a monochromatic Al Kα radiation at 1486.6 eV (225 W, 40 eV pass energy). The pressure in the spectrometer was typically $10^{-9}$ Torr. By combining low magnification (× 10) and a 2-mm aperture, an area ca. 0.2 mm in diameter was probed. Samples were held on a rectangular metal support by copper contact tape. Once the samples were introduced into the sample analysis chamber, they were manipulated in the *x*, *y*, and *z* directions and monitered by a CCD camera. Spatial measurements were referenced to the Au pads at the two ends of the 3 mm × 1 mm active gradient region. Fifteen equally separated spots along the 3-mm long active gradient region were chosen through software for XPS study. After subtraction of a linear background, all spectra were fit using 70% Gaussian/30% Lorentzian peaks, taking the minimum number of peaks consistent with the best fit.

**Atomic Force Microscopy (AFM).** AFM was performed on a Nanoscope III (Digital Instrument, Santa Barbara). The images were taken in tapping mode with 125-$\mu$m silicon tips (Nanodevices Metrology Probes, type TAP300, with a frequency of ∼300 kHz). The fast scan direction was from left to right. Scan rates for the experiments were typically 1 Hz.

**Surface Plasmon Resonance Imaging.** The apparatus for SPR imaging was adapted from a design published by Corn et al.[61] Light from a 100-W quartz-halogen bulb was focused and recollimated by a camera lens. The collimated light was passed through a polarizer and a narrow-band interference (830 nm band-pass, 10 nm fwhm) filter, illuminating the sample at the incident angle of interest. The reflected light was detected with a CCD camera and recorded on videotape. After digitizing the videotape, the image was analyzed employing Igor (Wavemetrics, Inc.).

**Flow Cell Assembly.** The flow cell assembly for SPR imaging has been described previously.[62] In brief, a Teflon cell was assembled with

(61) Nelson, B. P.; Frutos, A. G.; Brockman, J. M.; Corn, R. M. *Anal. Chem.* **1999**, *71*, 3928−3934.
(62) Zhang, Y.; Terrill, R. H.; Bohn, P. W. *Anal. Chem.* **1999**, *71*, 119−125.

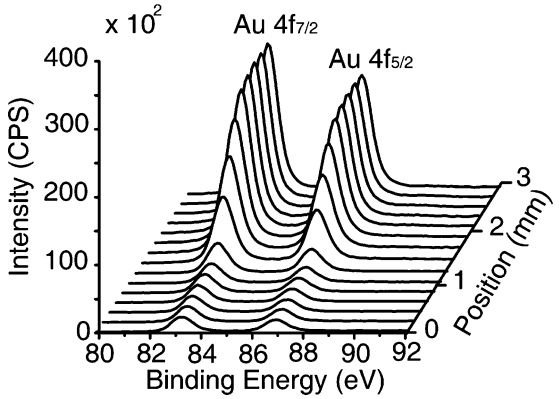


***Figure 2.*** X-ray photoelectron spectra of the Au 4f (80−92 eV) transition acquired from a PAA thickness gradient formed by DPG. Spectra were acquired at 15 equally separated positions along the sample length. The positions labeled 0 mm and 3 mm correspond to the negative end and positive end of the dynamic gradient, respectively.

the Au/prism as one side and a stainless steel plate (counter electrode) as the other, and the assembly was sealed by two O-rings (12.5-mm diameter). A Pt wire sealed into the cell through epoxy was attached to an external vessel containing a saturated Ag/AgCl reference electrode and electrolyte solution as a reference electrode.

## Results

**Fabrication of PAA Thickness Gradients.** PAA thickness gradients were formed on Au electrodes (Au-covered glass pieces and Au/prism) by electropolymerization[33−35] of 50:1 mole ratio (acrylic acid monomer)/(*N*,*N*′-methylenebisacrylamide cross-linker), in the presence of 0.2 M Zn(II). The electrochemically induced polymerization of acrylic acid was observed at positions corresponding to potentials more negative than ca. −1.1 V vs Ag/AgCl. The reaction results in the codeposition of Zn(0), which was removed either by applying a positive potential or by rinsing with dilute HCl. To generate laterally anisotropic PAA films, a bipotentiostat was used to establish an electrochemical potential gradient, $V(x)$, along the Au electrode surface. As shown in Figure 1a, the 150-nm thick Au pads at either end provide facile electrical connections, and their thickness ensures that the in-plane potential variation is largely confined to the narrow ultrathin ($d$ < 50 nm) film portion of the structure.[22] The potential gradient can be exploited to produce PAA film thickness gradients, because the magnitude of the local potential controls the rate of PAA electropolymerization (vide infra). PAA thickness gradients were fabricated using both SPG and DPG electrochemical potential programs. SPG was obtained by applying a constant in-plane potential gradient, typically setting ($E_1$, $E_2$) = (−1.3 V, −1.1 V), whereas DPG was created by applying a triangular potential sweep $E_1(t)$ while maintaining a constant potential offset, $\Delta = (E_2 - E_1)$, as shown in Figure 1b. Typically, $E_1$ was cycled between −1.5 and 0 V five times, keeping $\Delta = +300$ mV throughout the experiment. For both static and dynamic PAA gradients, the electrode surface was rinsed with 0.1 M HCl after PAA gradient film formation to ensure the complete removal of Zn(0).

**Characterization of PAA Gradients.** Figure 2 shows a series of spatially resolved XPS spectra of the Au 4f (80−92 eV) peaks acquired from 15 equally separated positions along the 3-mm-long active transition region of a PAA gradient formed by DPG on Au-covered glass. The position labeled 0 mm corresponds to the negative end of the dynamic gradient, and position 3 mm corresponds to the positive end. The intensities of Au 4f transitions gradually decrease going from the positive to the negative end because of differences in Au 4f signal attenuation along the electrode surface. For a Au electrode covered with a uniform PAA film of thickness $d$, the intensity of Au 4f signal can be written as:

$$I = I_o \exp(-d/\lambda) \tag{4}$$

where $I_o$ is the (unattenuated) signal from an infinitely thick bare Au electrode and $\lambda$ is the electron escape depth through the PAA film. The structural integrity of these films was assessed by performing tapping-mode AFM and SEM on a uniform thickness PAA film formed by sweeping potential between −1.5 and 0.0 V five times, then rinsing with 0.1 M HCl for 2 min. These data show a uniform pinhole-free film with rms roughness of 2.6 nm, over a 2.5 $\mu$m × 2.5 $\mu$m area, similar to the roughness of a freshly prepared Au substrate. Here $\lambda = 4.4$ nm is used, corresponding to the reported escape depth for 1400 eV electrons through poly(methyl methacrylate) (PMMA).[63] On the basis of this relationship, the PAA film thickness can be estimated if $I_o$ is known. In principle, $I_o$ can be estimated from a bare Au electrode in the same environment. However, bare Au surfaces prepared under the conditions utilized here are likely to be contaminated by an overlayer of adventitiously adsorbed material of unknown thickness. To achieve an accurate estimate for $I_o$, a bare Au electrode was derivatized with a self-assembled monolayer (SAM) of MUA. SAMs of MUA on evaporated Au have been thoroughly characterized by ellipsometry and ex-situ SPR measurements and found to be 1.7 nm thick.[63−65] Thus, the signal from an MUA-covered Au film was used to calibrate $I_o$ and thereby convert Au 4f XPS signals, $I(x)$, into PAA thicknesses, $d(x)$, as a function of position. Although there is likely some error in the absolute thickness values due to uncertainty in escape depth, the error affects all thickness values by the same ratio, leaving the form of the spatial distribution of PAA thicknesses, the relevant variable in this work, unaffected.

Figure 3 shows the thickness of PAA determined from eq 4 as a function of position. Clearly most of the thickness change occurs at positions corresponding to initial sweep potentials between −1.3 and −1.4 V, and a relatively steep gradient is obtained. The solid line is a fit of the experimental data to a sigmoidal function

$$d(x) = d_b + \frac{d_{max}}{1 + \exp[(x_0 - x)/r]} \tag{5}$$

where $d_b$ is a thickness offset, $d_{max}$ is the normalized maximum thickness, $x_0$ is the inflection point of the slope region, and $r$ is a spatial rate constant related to the slope. The width of the gradient, $W$, can be determined from the full width at half-maximum (fwhm) of the derivative of the fit function, $d'(x)$. The $x_0$ and $W$ values can be converted between potential and

(63) Tanuma, S.; Powell, C. J.; Penn, D. R. *Surf. Interface Anal.* **1994**, *21*, 165−176.
(64) Hanken, D. G.; Jordan, C. E.; Frey, B. L.; Corn, R. M. *Electroanal. Chem.* **1998**, *20*, 141−225.
(65) Bain, C. D.; Troughton, E. B.; Tao, Y. T.; Evall, J.; Whitesides, G. M.; Nuzzo, R. G. *J. Am. Chem. Soc.* **1989**, *111*, 321−335.

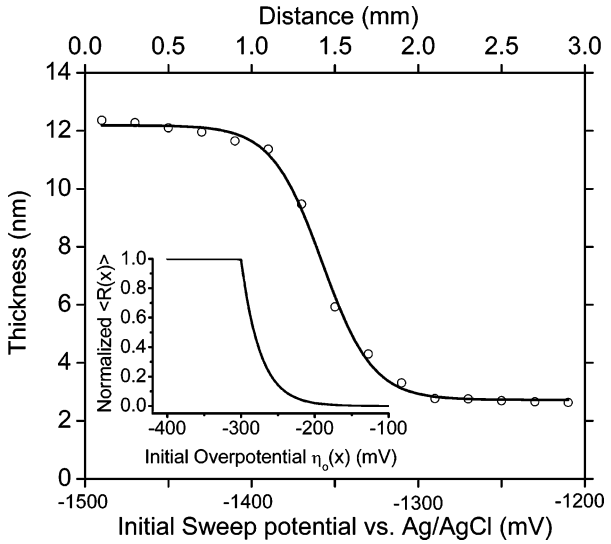


***Figure 3.*** Thickness of a PAA gradient formed by DPG, as determined from attenuation of the Au 4f signal, as a function of position or, equivalently, the initial potential value at $t_0$. The solid line is a fit to eq 5. The inset shows the form of the DPG thickness gradient calculated from eq 12.

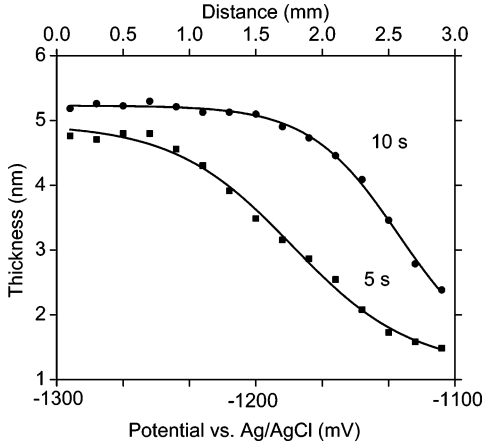


***Figure 4.*** Thickness of PAA gradients, as determined from attenuation of the Au 4f signal, as a function of position for gradients formed by SPG for 5 s (■) and 10 s (●). The solid lines are fits to eq 5.

physical space values using the width of the applied potential window, $\Delta V$, and the total length of the film.

Figure 4 shows the thickness profile of PAA gradients formed by SPG on Au-covered glass as a function of position and, thus, potential. The local thickness of the PAA film was determined from eq 4 and fits to the sigmoidal thickness function given in eq 5 were used to determine the transition region slopes. For the SPG PAA thickness gradient formed in 5 s, the PAA film thickness exhibits a transition in the potential region $-1250$ mV $< V(x) < -1150$ mV, with a width (fwhm of the derivative fit function) of 93 mV and a slope of 2.1 nm/mm. Then the 5 s PAA film thickness flattens out at potentials $V(x) < -1250$ mV. In contrast, the SPG PAA thickness gradient formed in 10 s changes PAA film thickness in the region $-1150$ mV $< V(x) < -1100$ mV with a width of 80 mV and a slope of 3.0 nm/mm. SPG gradients prepared with a variety of end potentials, ($E_1$, $E_2$), gave films in which the transition region could be placed at varying physical locations along the film length. However, as the data in Table 1 illustrate, the potential-space

***Table 1.*** PAA Thickness Transition Region under SPG Formation Conditions[a]

| ($E_1$, $E_2$) (V) | transition potential (V)[b] |
|---|---|
| (−1.3, −0.7) | −1.16 ± 0.01 |
| (−1.3, −0.8) | −1.17 ± 0.01 |
| (−1.3, −0.9) | −1.18 ± 0.01 |
| (−1.3, −1.0) | −1.15 ± 0.01 |
| (−1.3, −1.1) | −1.19 ± 0.01 |
| (−1.25, −0.95) | −1.12 ± 0.01 |
| (−1.35, −1.05) | −1.16 ± 0.01 |
| (−1.4, −1.1) | −1.13 ± 0.01 |

[a] Gradients were generated by 1 min. electrolysis. [b] Transition regions were determined by optical microscopy prior to zinc removal.

locations of the transition region, derived from eq 5, vary only slightly from film to film.

SPR imaging, because it reports on the spatial distribution of the optical response function, can provide information about SPG- and DPG-derived PAA thickness gradients complementary to that obtained from XPS profiling. Imaging was performed with an incoherent white light source/narrow band interference filter combination,[66] at an incident angle corresponding to the minimum reflectance angle for bare Au. Figure 5a shows the SPR image of a DPG-derived PAA thickness gradient formed with the negative end swept from $-1300$ mV to $+100$ mV once at 50 mV/s, while maintaining an offset of $\Delta = -200$ mV relative to the positive electrode. Figure 5b is a reflectivity profile of the image in Figure 5a. Figure 5a,b shows very little reflectance change at positions corresponding to initial potentials, $V(x,t = 0) > -1125$ mV, and then the reflectance increases gradually with more negative initial potentials in the range $-1125$ mV $> V(x,t = 0) > -1280$ mV. Because the images are acquired at the angle of the SPR resonance for bare Au, $\theta_{\mathrm{min,Au}}$, lighter regions correspond to spatial locations where the resonance position has shifted from its bare Au position. In light of the XPS data it is reasonable to infer that the shift results from the formation of PAA, so that lighter regions correspond to thicker PAA layers. The key feature of these data is the relatively gradual transition between low and high reflectance for the DPG-derived film. For comparison, a PAA thickness gradient generated by SPG with ($E_1$, $E_2$) = (−1.3 V, −1.1 V) for 5 s and imaged with SPR, is shown in Figure 5c,d. The static gradient exhibits little reflectance change until positions just negative of −1.1 V. Then the reflectance begins to increase with more negative potential until there is a relatively sharp transition at positions corresponding to potentials $-1150$ mV $> V(x) > -1175$ mV. As a whole, the transition region for the SPG-derived PAA film is much sharper than that for the DPG-derived film.

## Discussion

**Gradient Formation Mechanism.** The electropolymerization reactions studied here form PAA gradients under fundamentally different constraints than the monolayer composition gradients that have been studied previously.[5,6,16,19−23,67] Whereas thiol SAM-based monolayer composition gradients are limited to single molecule thick coverages, the PAA films fabricated here can, in principle, be grown to arbitrary thickness. Furthermore, whereas the SAM thiol composition gradients are achieved by

(66) Brockman, J. M.; Nelson, B. P.; Corn, R. M. *Annu. Rev. Phys. Chem.* **2000**, *51*, 41−63.
(67) Wang, Q.; Bohn, P. W. *J. Phys. Chem. B* **2003**, *107*, 12578−12584.

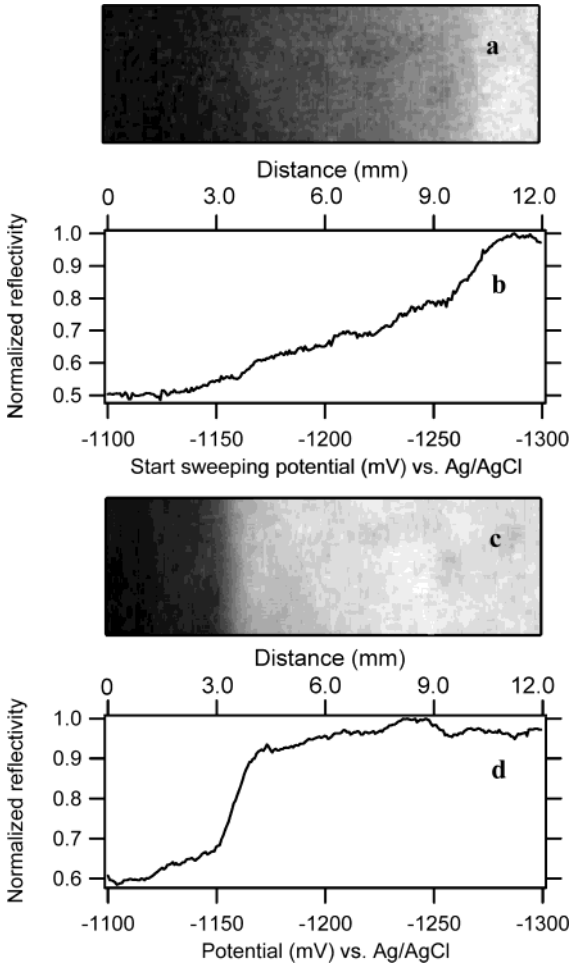


***Figure 5.*** (a) SPR image acquired at 830 nm of a PAA gradient formed by DPG with the negative end swept from −1300 mV to +100 mV once at 50 mV/s while maintaining an offset of $\Delta = +200$ mV at the positive electrode. (b) Normalized reflectivity profile of the image in (a). (c) SPR image acquired at 830 nm of a PAA gradient formed by SPG with ($E_1$, $E_2$) = (−1.3 V, −1.1 V) for 5 s. (d) Normalized reflectivity profile of the image in (c).

thermodynamic control over the local adsorbed population, the thickness gradients studied here are produced under kinetic control. Two kinetic regimes can be identified. (1) Under conditions where the rate of monomer incorporation is rate-limiting, the local PAA thickness, $d(x)$, is determined by the rate of polymerization at a given location, $R(x,t)$, integrated over the time in which electropolymerization takes place. The rate constant is expressed as a function of both space and time to recognize the DPG polymerization protocol explicitly. (2) If the rate becomes sufficiently fast that the incorporation rate is controlled by the rate of monomer delivery to the growing interface, then mass transport controls the rate of film thickness extension. The transition between these two regimes can be stated in terms of a threshold potential, $V_{\text{thresh}}$, as

$$d(x) = \kappa \int_0^{t_p} R(x, t)dt; \quad \{x:\ V(x) < V_{\text{thresh}}\}$$

$$d(x) = \kappa R_{\max} t_p; \quad \{x:\ V(x) \geq V_{\text{thresh}}\} \qquad (6)$$

where $\kappa$ is a constant to convert reaction rate into film thickness and $t_p$ is the polymerization time. The second equation, which describes the mass transport-limited regime, is strictly true only at short electropolymerization times, such as those studied here, because the formation of the insulating PAA film naturally limits the rate at which electron transfer can occur.

The overall rate, $R(x,t)$, depends on the rate constant, $k(x,t)$, which is dependent on the local potential through the Butler−Volmer equation, which gives the rate constant for electron transfer as a function of the overpotential, $\eta(x,t)$

$$k(x, t) = k^0 \exp(-\alpha n f \eta(x,t)) \approx k^0(1 - \alpha n f \eta(x, t)) \qquad (7)$$

where $\alpha$ is the transfer coefficient, $n$ is the number of electrons participating in the reaction, and $f = F/RT$ collects the Faraday constant, $F$, and the thermal energy. The minus sign results from the fact that negative overpotentials correspond to enhanced polymerization rates.

**PAA Gradients Formed by SPG.** Electropolymerizing in the presence of an SPG in-plane electrochemical potential gradient results in a position-dependent overpotential, $\eta(x)$, so that the rate constant, $k(x)$, and thus the rate, $R(x)$, depend on position only, not position and time. Equation 7 obviously predicts an overall exponential dependence of rate on overpotential. However, if the overpotential at which mass transport becomes limiting is small ($\eta \rightarrow 0$), then the linear approximation indicated in the second part of eq 7 can be used. Assuming that the rate law for AA electropolymerization follows that of polyacrylamide[33] and allowing for position-dependent potentials

$$\begin{aligned} R(x) &= k(x)[\text{Zn}^{2+}]^{1/2}[\text{AA}] \\ &= k^0 \exp(-\alpha n f \eta(x))[\text{Zn}^{2+}]^{1/2}[\text{AA}] \\ &\approx k^0(1 - \alpha n f \eta(x))[\text{Zn}^{2+}]^{1/2}[\text{AA}] \quad \{\text{small } \eta \text{ limit}\} \end{aligned} \qquad (8)$$

At short reaction times it is reasonable to assume that the solution concentrations of starting materials do not change appreciably and that the effects of forming an insulating PAA film are not too severe. Thus, in the limit of small overpotentials, eq 8 predicts that $R(x)$ is a linear function of $\eta(x)$, and consequently, eq 6 predicts that the film thickness at a given location, $d(x)$, grows linearly in time at a rate determined by the local overpotential, $\eta(x)$.

Three salient features of the SPG-formed PAA thickness gradients deserve comment: the relationship of thicknesses determined by SPR imaging and XPS, the variation of the saturation thickness with polymerization time, and the sharpness of the transition region compared to DPG-derived films. The transition region of the 5 s SPG PAA thickness gradient as determined from SPR imaging, Figure 5c,d is sharper than that determined by XPS (Figure 4). This is because SPR imaging provides in situ PAA film thickness information, while XPS naturally addresses the dry PAA film. Hydrogels, such as PAA, are hydrophilic network polymers that can swell and hold a large amount of water while maintaining their structure.[68] Thus, wet films are expected to be much thicker. In addition, there is no a priori reason to expect a linear relationship between the wet and dry PAA film thicknesses, which further complicates comparison of PAA thicknesses determined from XPS and SPR imaging. Clearly the XPS data provide a quantitative report of the thickness profile in the dry state, while the SPR images provide a qualitative picture of the hydrated films.

(68) Peniche, C.; Cohen, M. E.; Vazquez, B.; SanRoman, J. *Polymer* **1997**, *38*, 5977−5982.

The second interesting feature of the SPG data is that the 10 s static gradient produces an anisotropic PAA film with a steeper slope in the transition region than that produced from a 5 s static gradient. Since eq 8 predicts that $R(x)$ is a linear function of $\eta(x)$, the film thickness at a given location, $d(x)$, grows linearly in time at a rate determined by the local overpotential, $\eta(x)$. If the spatial slope of the in-plane electrochemical potential gradient, $d\eta/dx$, is fixed, as it is in SPG-derived films, then the observed PAA thickness gradient must have a steeper slope at longer growth times, because a larger change in thickness is obtained over the same spatial region. The larger change in thickness results from the fact that, in the mass transport-limited region of the film, eq 6 predicts a larger film thicknesses at longer polymerization times.

**PAA Gradients Formed by DPG.** Gradients formed by DPG differ fundamentally from those formed by SPG in that $\eta(x,t)$, and therefore $k(x,t)$ and $R(x,t)$, vary in both space and time. Figure 3 illustrates that PAA films produced by DPG can be divided into three sections. In the region corresponding to initial sweep potentials, $-1200$ mV $> V(x,t = 0) > -1300$ mV, the PAA film thickness does not change; in the region $-1300$ mV $> V(x,t = 0) > -1400$ mV, the PAA film thickness increases with more negative initial sweep potentials; and when the initial sweep potential is more negative than $-1400$ mV, the PAA film thickness reaches a limiting value due to mass transport control, as discussed above.

Setting aside the mass transport-controlled region and considering only those areas controlled by the local overpotential, PAA growth by DPG can be thought of as an accumulation of a series of overlapping SPG gradients. For a given position with starting overpotential $\eta_0(x)$, the final film thickness is determined by the average rate of polymerization, which is

$$\langle R(x)\rangle = \frac{\gamma}{t_p}\int_0^{t_p} k(x,t)\,dt \tag{9}$$

where $\gamma = [Zn^{2+}]^{1/2}[AA]$ accounts for the nearly static solution reactant concentrations. In turn, $k(x,t)$ can be written

$$k(x,t) = k^0 \exp[-\alpha n f \eta(x,t)] \tag{10}$$

and

$$\eta(x,t) = \eta_0(x) - st \tag{11}$$

where $s = dV/dt$ is the scan rate in the DPG protocol. Combining eqs 9−11 yields

$$\langle R(x)\rangle = \frac{\gamma k^0}{\alpha n f s t_p}[\exp(\alpha n f s t_p) - 1][\exp(-\alpha n f \eta_0(x))] \tag{12}$$

Clearly the local PAA film thickness is controlled by the final exponential term. Thus, the predicted spatial thickness profiles have the same shape as those obtained with SPG, although with different slope, because of the difference in the pre-exponential factors in eqs 8 and 12. All that remains is to couple the linear portion of the thickness profile with a mass transport-limited regime analogous to eq 6 to recover the PAA gradient profile as shown in the Figure 3 inset. Experimentally DPG-derived PAA gradients are observed to be spatially broader than similar SPG-derived gradients with the same initial potential and comparable effective growth time, cf. Figure 5b,d.

On the basis of the analysis above, the PAA gradient properties, such as slope and limiting thickness, depend on growth time. With longer growth time, SPG-derived PAA gradients become steeper and thicker. However, if the growth time is too long, Zn(0) will build up on the electrode surface, possibly invalidating the linear potential variation along the electrode surface. On the other hand, Zn(0) should, in principle, not accumulate in the DPG-derived PAA gradients, because Zn(0) formed at positions corresponding to negative potentials can be reoxidized and dissolved when the local potential sweeps to a more positive values. DPG is, thus, the preferred route to thicker PAA gradient formation, in which, according to eq 12, the properties of the dynamic gradient such as slope and size can be tuned by adjusting initial sweep potential and range, sweep rate, and cycle times.

## Conclusion

PAA thickness gradients have been mapped onto Au electrodes through electropolymerization of acrylic acid using both static and dynamic electrochemical potential gradients. These laterally anisotropic films represent a new type of in-plane electrochemical gradient structure, in which the nominal composition is constant, while a physical property, i.e., PAA film thickness, varies with position. In contrast to electrochemically derived composition gradients, the PAA film thickness is controlled primarily by electropolymerization kinetics. At small absolute overpotentials and short growth times, the lateral thickness distribution, $d(x)$, of PAA films prepared by SPG is well-described by the Butler−Volmer equation. At more negative overpotentials, mass transport limits the rate of electropolymerization, and the film grows at a constant rate, independent of local potential. Because the spatial location corresponding to $V_{thresh}$ is, to first order, fixed in SPG-derived films, the slope of the film thickness gradient is related to the time of polymerization or these films. PAA gradient films produced by DPG can be regarded as an accumulation of a series of overlapping static PAA gradients with a shifted transition region. The $d(x)$ for DPG-derived PAA gradients are well-described by a temporally integrated form of the Butler−Volmer equation. Equation 12 predicts a different slope in the transition region for DPG- vs SPG-derived gradient films, which is indeed observed. The key operational difference between SPG and DPG PAA gradients is the excursion to positive potentials at all film locations during specific parts of the triangular voltage sweep for DPG. Exposing the growing electropolymerized PAA film to positive potentials aids in removal of Zn(0), resulting in thicker PAA films by DPG.

One application of these anisotropic in-plane PAA thickness gradients involves the preparation of artificial cell adhesion surfaces with extracellular matrix mimics, e.g., peptides containing the Arg-Gly-Asp sequence,[23] in such a way that both chemical (RGD content) and physical (thickness) properties of the surfaces may be varied to study cellular adhesion and motility. Thickness gradients may also be exploited in sensing modalities employing a spatially continuous readout. The utility of angle-dependent SPR measurements is illustrated in Figure 5. If instead wavelength-dependent SPR measurements are made, each position corresponds to a unique thickness, $d(x)$,

and produces a unique SPR resonance wavelength, $\lambda_{SPR}(x)$. Challenging such a structure with analytes transported orthogonal to the thickness gradient axis would then allow local changes in $\lambda_{SPR}(x)$ to be read out by imaging. Thickness changes could be induced by swelling−deswelling transitions in the volume of the PAA[69] to induce local changes in $\lambda_{SPR}(x)$, or changes in optical coupling to Au nanoparticles immobilized to the PAA surface could be induced by molecular recognition motifs bound to the surface of the Au particles.[70]

**Acknowledgment.** This work was supported by the Department of Energy through Grant 91ER45439. We thank Dr. Rick Haasch of the Frederick Seitz Materials Research Laboratory for his assistance with the small-area XPS measurements.

JA0400436

(69) Yu, Q.; Bauer, J. M.; Moore, J. S.; Beebe, D. J. *Appl. Phys. Lett.* **2001**, *78*, 2589−2591.
(70) He, L.; Musick, M. D.; Nicewarner, S. R.; Salinas, F. G.; Benkovic, S. J.; Natan, M. J.; Keating, C. D. *J. Am. Chem. Soc.* **2000**, *122*, 9071−9077.